

**STATIC H_∞ CONTROL OF A CANTILEVERED BEAM USING
AN ANALYTICAL UPPER BOUND APPROACH**

By

Robert John Sweeney

A Thesis
Submitted to the Faculty
of the

WORCESTER POLYTECHNIC INSTITUTE

In partial fulfillment of the requirements for the

Degree of Master of Science

In

Mechanical Engineering
By

May 2005

APPROVED:

Professor Michael A. Demetriou (Advisor)

Professor Karolos Grigoriadis, Committee Member

Professor Zhikun Hou, Committee Member

Professor Mark Richman, Committee Member

Professor Nikos Gatsonis, Graduate Committee Representative

Abstract

This paper considers the H_∞ control of externally symmetric vector second order systems using an analytical upper bound method. The structural model is a cantilevered aluminum beam with a collocated pair of piezoceramic patches to serve as actuators and sensors. A computationally efficient method for approximating the H_∞ norm for externally symmetric systems is presented. The approximation method is then used to calculate a scalar output feedback controller to guarantee a closed-loop H_∞ norm less than any user defined value. This method is tested with a finite-element representation of the beam, and then verified experimentally.

Acknowledgements

I would like to take this opportunity to thank my advisor Professor Michael Demetriou for his guidance in both academics and in life.

I would like to thank my mother and father for their constant love and support, and I would like to thank my sister Meghan and brother Billy whose friendship I will forever cherish.

Table of Contents

Table of Contents	iii
Table of Figures	iv
List of Tables	v
Nomenclature	vi
1 Introduction	1
2 Dynamic Modeling	1
2.1 The Weak Form	2
2.2 The Galerkin Method	3
2.3 Cubic Splines	5
2.4 Applying Type I and Type II Boundary Conditions	8
2.5 Natural Frequencies and Modeshapes	9
3 Solving the Eigenvalue Problem With Modal Analysis	11
4 Controllability and Placement of Piezos	13
4.1 Forcing Due to Piezos	13
4.2 Controllability	14
5 Response to Forcing	16
5.1 Impulse Response	16
5.2 Duhamel's Integral	18
5.3 Response From Impact Hammer	19
6 Damping	20
7 Modeling Damping in the Frequency Domain	21
8 The Control Synthesis Problem	22
8.1 Feedback From the PZT	23
8.2 Feedback Control Law	24
8.3 Simulated Results	25
9 Experimental Verification	29
9.1 Experimental Results	32
10 Conclusions	34

Table of Figures

Figure 2-1	3
Figure 2-2: Cubic Spline Centered at 0 with $h=1$	7
Figure 2-3: Distribution of Splines for a Beam of Five Elements	7
Figure 2-4: First Four Modeshapes	11
Figure 4-1: Trace of P vs. Center of Piezo.....	15
Figure 5-1: Force vs. Time.....	18
Figure 5-2: Force From Hammer	19
Figure 5-3: Response From Impact Hammer.....	20
Figure 7-1: Experimental and Computational Frequency Response	22
Figure 8-1: Closed Loop Frequency Response $\gamma = 10$	26
Figure 8-2: Closed Loop Frequency Response $\gamma = 1$	26
Figure 8-3: Closed Loop Frequency Response $\gamma = 0.01$	27
Figure 8-4: Magnitude plots using dynamic and static controllers $\gamma = 1.5$	28
Figure 9-1: Analog Differentiator DC Gain -40dB.....	29
Figure 9-2: Magnitude Response of Analog Differentiator	30
Figure 9-3: Phase Response of Analog Differentiator	30
Figure 9-4: Schematics for the Apparatus	31
Figure 9-5: The Cantilevered Beam.....	32
Figure 9-6: dSPACE 1103 Rapid Prototyping Board + Differentiator.....	32
Figure 9-7: Open Loop and Closed Loop Magnitude Response $G = 0.055268$ (Experimental)	33
Figure 9-8: Open Loop and Closed Loop Magnitude Response $G = 0.055268$ (Computational 40 Elements)	33

List of Tables

Table I: Table of Natural Frequencies	9
Table II: Computation Time for Calculating the True Infinity Norm vs. (8.10) $n=120$...	27
Table III: Computation Time for Dynamic and Static Controllers for $\gamma = 1.5$	29

Nomenclature

A^T	Transpose of A
A^+	Moore-Penrose Generalized Inverse of A
A^\perp	Left Null Space of A
x	State Vector of x
X	Eigenvector of x
G	Static Feedback Gain

1 Introduction

The purpose of this paper is to develop a computationally efficient method for the H_∞ control design of systems with externally symmetric transfer functions. Control of the H_∞ norm is a widely used and highly effective method for vibration attenuation, but requires intense computational power both online and offline. The dynamic full-state observer based H_∞ controller uses a bisection iteration method [2] for calculating the H_∞ norm offline and uses a full-state observer online to estimate the instantaneous state. This puts limitations on the sample rate for the real time code and precludes observation of high order modes.

In this paper, an alternative method is proposed for systems that have the special property of *external symmetry*. If a transfer function is symmetrical in its first order state-space form

$$\begin{aligned}\dot{x} &= Ax + Bu \\ y &= Cx + Du \\ C &= B^T \\ D &= 0\end{aligned}$$

the H_∞ norm can be approximated using an analytical upper bound method. A control law in the form of $u = -Gy$ will render the H_∞ norm of the closed loop transfer function bound by any user-defined value.

2 Dynamic Modeling

To simulate the vibrations of a cantilever beam, we start with the well-known partial differential equation

$$\frac{\partial^2}{\partial x^2} \left(EI \frac{\partial^2 y}{\partial x^2} \right) + \rho A \frac{\partial^2 y}{\partial t^2} = f(x, t) \quad (2.1)$$

where y represents the axial displacement, x is the location along the length of the beam, E is the elastic modulus, I is the area moment of inertia, A is the cross sectional area and ρ is the density of the beam. The forcing function $f(x, t)$ is a force density with units of N/m . Analytically; assuming the solution is separable with space and time can solve this partial differential equation

$$y = \sum_{j=1}^{\infty} \phi_j(x) \alpha_j(t) \quad (2.2)$$

where $\phi_i(x)$ is a function only of x and $\alpha_i(x)$ is a function only of t . The partial differential equation can then be approximated by an ordinary differential equation, which can easily be solved using conventional techniques.

For this project, however, we will approximate a solution using the weak form of the equation and employ a finite elements methods to generate the mass and stiffness matrices.

2.1 The Weak Form

The solution of (2.1) is assumed to be as follows

$$y = \sum_{j=1}^N \phi_j(x) \alpha_j(t) \quad (2.3)$$

where N is a finite integer. We assume as in the analytic case that ϕ_j is a function only of x and α_j is a function only of t . We can then substitute this approximate solution into (2.1) assuming E and I are constant throughout the beam.

$$EI \sum_{j=1}^N \phi_j^{(4)} \alpha_j + \rho A \sum_{j=1}^N \phi_j \ddot{\alpha}_j = f(x, t) + R_j \quad (2.4)$$

where R_j is the residual error arising from the approximation (2.3)

2.2 The Galerkin Method

Now that the equation is in weak form, we can use a finite elements method to approximate the solution. First the beam is divided into many small elements.

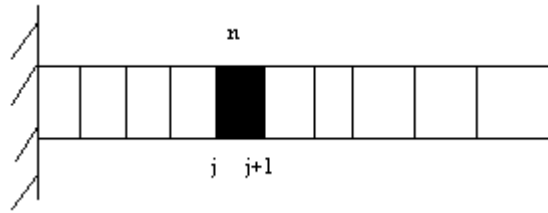


Figure 2-1

The nth element of the beam is shown in Figure 2-1, which is bounded, by nodes j and $j+1$. For a beam of N nodes, the solution $y(x, t)$ is approximated by (2.3). We now put (2.4) in the following form

$$EI \sum_{j=1}^N \phi_j^{(4)} \alpha_j + \rho A \sum_{j=1}^N \phi_j \ddot{\alpha}_j - f(x, t) = R_j$$

and force all residuals R_j to be orthogonal to all basis functions ϕ_j . To do this we take the inner product of R_j and ϕ_i and set the result to zero.

$$\int_0^L R_j \phi_i dx = EI \sum_{j=1}^N \alpha_j \int_0^L \phi_j^{(4)} \phi_i dx + \rho A \sum_{j=1}^N \ddot{\alpha}_j \int_0^L \phi_j \phi_i dx - f(x, t) \int_0^L \phi_i dx = 0 \quad (2.5)$$

for $i = 1 \dots N$. The result is a system of N equations which is written in matrix form

$$\begin{aligned}
& EI \begin{bmatrix} \int_0^L \phi_1^{(4)} \phi_1 dx & \int_0^L \phi_2^{(4)} \phi_1 dx & \dots & \int_0^L \phi_N^{(4)} \phi_1 dx \\ \int_0^L \phi_1^{(4)} \phi_2 dx & \int_0^L \phi_2^{(4)} \phi_2 dx & \dots & \vdots \\ \vdots & \vdots & \ddots & \int_0^L \phi_N^{(4)} \phi_{N-1} dx \\ \int_0^L \phi_1^{(4)} \phi_N dx & \dots & \int_0^L \phi_{N-1}^{(4)} \phi_N dx & \int_0^L \phi_N^{(4)} \phi_N dx \end{bmatrix} \begin{Bmatrix} \alpha_1 \\ \alpha_2 \\ \vdots \\ \alpha_{N-1} \\ \alpha_N \end{Bmatrix} \\
& + \rho A \begin{bmatrix} \int_0^L \phi_1 \phi_1 dx & \int_0^L \phi_2 \phi_1 dx & \dots & \int_0^L \phi_N \phi_1 dx \\ \int_0^L \phi_1 \phi_2 dx & \int_0^L \phi_2 \phi_2 dx & \dots & \vdots \\ \vdots & \vdots & \ddots & \int_0^L \phi_N \phi_{N-1} dx \\ \int_0^L \phi_1 \phi_N dx & \dots & \int_0^L \phi_{N-1} \phi_N dx & \int_0^L \phi_N \phi_N dx \end{bmatrix} \begin{Bmatrix} \ddot{\alpha}_1 \\ \ddot{\alpha}_2 \\ \vdots \\ \ddot{\alpha}_{N-1} \\ \ddot{\alpha}_N \end{Bmatrix} = \begin{Bmatrix} \int_0^L \phi_1 f(x,t) dx \\ \int_0^L \phi_2 f(x,t) dx \\ \vdots \\ \int_0^L \phi_{N-1} f(x,t) dx \\ \int_0^L \phi_N f(x,t) dx \end{Bmatrix}
\end{aligned} \tag{2.6}$$

Equation 2.6 is now written as

$$M\ddot{x} + Kx = B_0 \tag{2.7}$$

where

$$\begin{aligned}
M &= \begin{bmatrix} \int_0^L \phi_1 \phi_1 dx & \int_0^L \phi_2 \phi_1 dx & \dots & \int_0^L \phi_N \phi_1 dx \\ \int_0^L \phi_1 \phi_2 dx & \int_0^L \phi_2 \phi_2 dx & \dots & \vdots \\ \vdots & \vdots & \ddots & \int_0^L \phi_N \phi_{N-1} dx \\ \int_0^L \phi_1 \phi_N dx & \dots & \int_0^L \phi_{N-1} \phi_N dx & \int_0^L \phi_N \phi_N dx \end{bmatrix} \\
K &= \begin{bmatrix} \int_0^L \phi_1^{(4)} \phi_1 dx & \int_0^L \phi_2^{(4)} \phi_1 dx & \dots & \int_0^L \phi_N^{(4)} \phi_1 dx \\ \int_0^L \phi_1^{(4)} \phi_2 dx & \int_0^L \phi_2^{(4)} \phi_2 dx & \dots & \vdots \\ \vdots & \vdots & \ddots & \int_0^L \phi_N^{(4)} \phi_{N-1} dx \\ \int_0^L \phi_1^{(4)} \phi_N dx & \dots & \int_0^L \phi_{N-1}^{(4)} \phi_N dx & \int_0^L \phi_N^{(4)} \phi_N dx \end{bmatrix}
\end{aligned}$$

and

$$B_0 = \left\{ \begin{array}{c} \int_0^L \phi_1 f(x,t) dx \\ \int_0^L \phi_2 f(x,t) dx \\ \vdots \\ \int_0^L \phi_{N-1} f(x,t) dx \\ \int_0^L \phi_N f(x,t) dx \end{array} \right\}$$

Now that there is a method for us to generate the mass and stiffness matrices, it remains to choose an appropriate basis function $\phi(x)$.

2.3 Cubic Splines

We must choose an appropriate basis function in order to get accurate results. Firstly, we recognize that M must be a positive definite, symmetric matrix, therefore $\phi(x)$ must be positive for all x . We also recognize from K the fourth order derivative. This tells us that $\phi(x)$ must also be at least twice differentiable. It may seem at first glance that $\phi(x)$ must be *four* times differentiable, however we will use the technique of integration by parts to circumvent this constraint. Integration by parts also gives us a vehicle in which to apply our moment and shear force boundary conditions. If we integrate the term

$\int_0^L \phi_j^{(4)} \phi_i dx$ by parts we arrive at $\int_0^L \phi_j^{(4)} \phi_i dx = \left[\phi_j''' \phi_i \right]_0^L - \int_0^L \phi_j''' \phi_i' dx$. By observing that in

cantilever beams $\phi_j'''(L) = 0$ and $\phi_i(0) = 0$ we can eliminate the first term and the

integral reduces to $\int_0^L \phi_j^{(4)} \phi_i dx = - \int_0^L \phi_j''' \phi_i' dx$. We can integrate again by parts and arrive

at $\int_0^L \phi_j^{(4)} \phi_i dx = - \left(\left[\phi_i' \phi_j'' \right]_0^L - \int_0^L \phi_i'' \phi_j'' dx \right)$. We now observe that in our case $\phi_j''(L) = 0$

and $\phi_i'(0) = 0$ thus the integral reduces to

$$\int_0^L \phi_j^{(4)} \phi_i dx = \int_0^L \phi_i'' \phi_j'' dx \quad (2.8)$$

Since there are no derivatives of higher order than two in (2.8), the basis function need only be twice differentiable, and the moment and sheer force boundary conditions have already been applied. In light of these observations, a simple basis function to choose would be the cubic spline [7]. It is twice differentiable, positive for all x and has the convenient property that it is nonzero only within a small interval of space. This property will simplify the calculation of the mass and stiffness matrices greatly because it will force most of the terms to be zero, and the final result will be a banded matrix with a bandwidth of 9.

The splines are piecewise smooth cubic functions symmetric about the mean. The maximum value of the splines occurs at the mean and has a maximum value of 4. Mathematically, the splines have the following form:

$$\phi_j(x) = \frac{1}{h^3} \begin{cases} 0 & x \leq x_c - 2h \\ (x + 2h - x_c)^3 & x_c - 2h < x \leq x_c - h \\ h^3 + 3h^2(x + h - x_c) + 3h(x + h - x_c)^2 - 3(x + h - x_c)^3 & x_c - h < x \leq x_c \\ h^3 + 3h^2(x_c - x + h) + 3h(x_c + h - x)^2 - 3(x_c + h - x)^3 & x_c < x \leq x_c + h \\ (x_c + 2h - x)^3 & x_c + h < x \leq x_c + 2h \\ 0 & x \geq x_c + 2h \end{cases} \quad (2.9)$$

where x_c is the center of the spline and h is the space between the nodes in an element.

When $x_c = 0$ and $h = 1$, $\phi(x)$ looks like

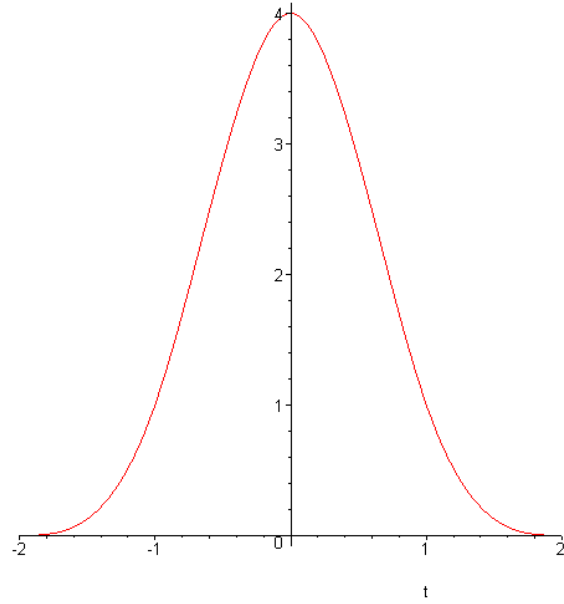


Figure 2-2: Cubic Spline Centered at 0 with $h=1$

For a beam that is divided into five elements, the cubic splines will be distributed as shown in Figure 2-3

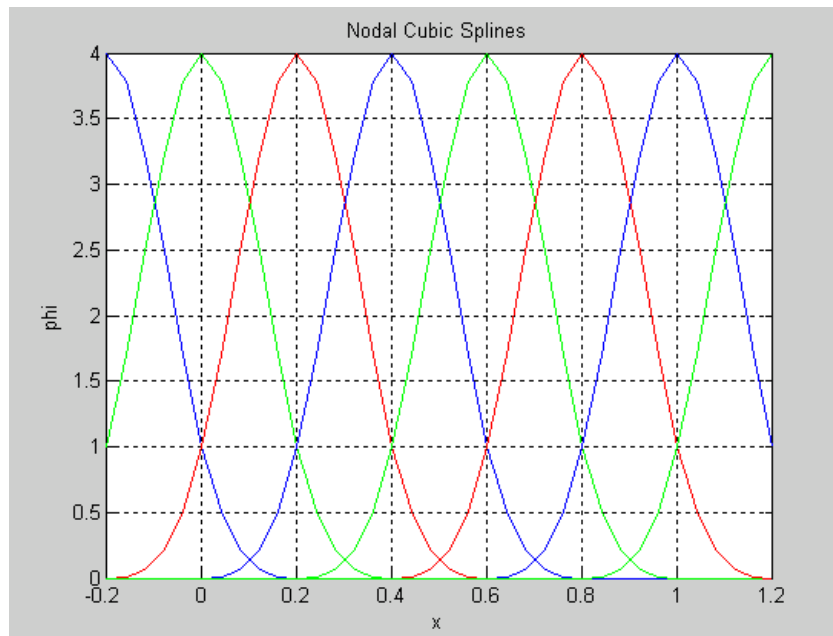


Figure 2-3: Distribution of Splines for a Beam of Five Elements

2.4 Applying Type I and Type II Boundary Conditions

Now that the basis function has been clearly defined, we must take care of the boundary conditions at the root of Type I. Both the displacement and the slope must equal zero at $x=0$. We have two methods of applying these boundary conditions. The most direct method is to eliminate the first row and column of the mass and stiffness matrix. This simply acknowledges that the node at zero is irrelevant and we need not consider it. This method is somewhat crude and awkward. We will use a much smoother method that will apply the boundary conditions as well as providing a method to model other beams of different support structures rather simply. We will modify the basis function such that the slope and displacement are zero at $x=0$. Noting that the displacement at $x=0$ is

$$\begin{aligned} y(t, 0) &= \alpha_1 \phi_1(0) + \alpha_2 \phi_2(0) + \alpha_3 \phi_3(0) + \dots + \alpha_N \phi_N(0) \\ &= \alpha_1 + 4\alpha_2 + \alpha_3 \end{aligned}$$

If we make $\alpha_1 = -2$, $\alpha_2 = 1$ and $\alpha_3 = -2$, $y(t, 0) = 0$. Similarly,

$$\begin{aligned} y'(t, 0) &= \alpha_1 \phi_1'(0) + \alpha_2 \phi_2'(0) + \alpha_3 \phi_3'(0) + \dots + \alpha_N \phi_N'(0) \\ &= \frac{3}{h} \alpha_1 + 0 - \frac{3}{h} \alpha_3 = -\frac{6}{h} + 0 + \frac{6}{h} \alpha_3 = 0 \end{aligned}$$

Thus if we introduce the transformation matrix T

$$T = \begin{bmatrix} -2 & 1 & -2 & 0 & \dots & 0 \\ 0 & 0 & 0 & 1 & \dots & 0 \\ \vdots & 0 & \dots & 0 & \ddots & 0 \\ 0 & 0 & \dots & 0 & 0 & 1 \end{bmatrix} \quad (2.10)$$

and premultiply it with the vector of basis functions we arrive at a modified set of $N-2$ basis functions, which satisfy all boundary conditions.

$$\begin{bmatrix} \psi_1 \\ \psi_2 \\ \vdots \\ \psi_{N-2} \end{bmatrix} = T \begin{bmatrix} \phi_1 \\ \phi_2 \\ \vdots \\ \phi_N \end{bmatrix} \quad (2.11)$$

We now can numerically integrate (2.6) and generate the mass and stiffness matrices using the Matlab program FEM_mode*.

At the free-end, the second and third order derivatives must be set to zero. This condition is satisfied through the integration by parts of the inner product (see section 2.3).

2.5 Natural Frequencies and Modeshapes

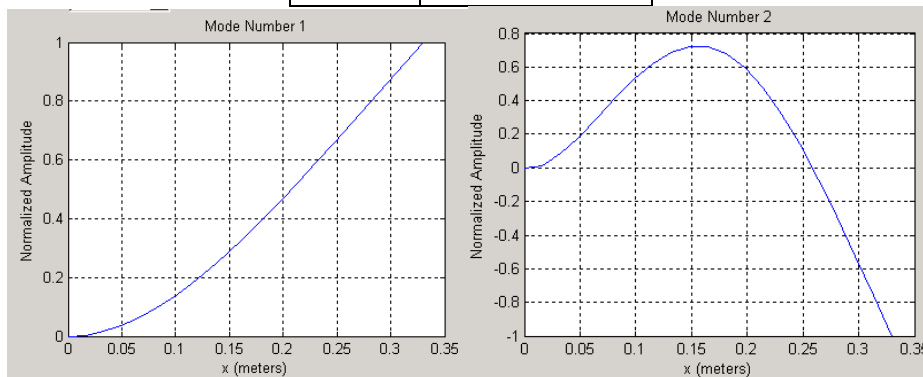
Using the program FEM_mode, the following natural frequencies were calculated for a beam of length 0.330 meters, stiffness 6.89e10 Pa, density 2730 kg/m³, thickness 0.0015494 meters, and width 0.0508 meters with 20 elements:

Table I: Table of Natural Frequencies

Mode	Frequency (rad/s)
1	72.736
2	454.66
3	1272.9
4	2494.5
5	4123.8
6	6161.6

* Written by author

7	8609.4
8	11471
9	14754
10	18469
11	22637
12	27289
13	32473
14	38249
15	44684
16	51806
17	59513
18	67410
19	74640
20	79898
21	2.27E+05



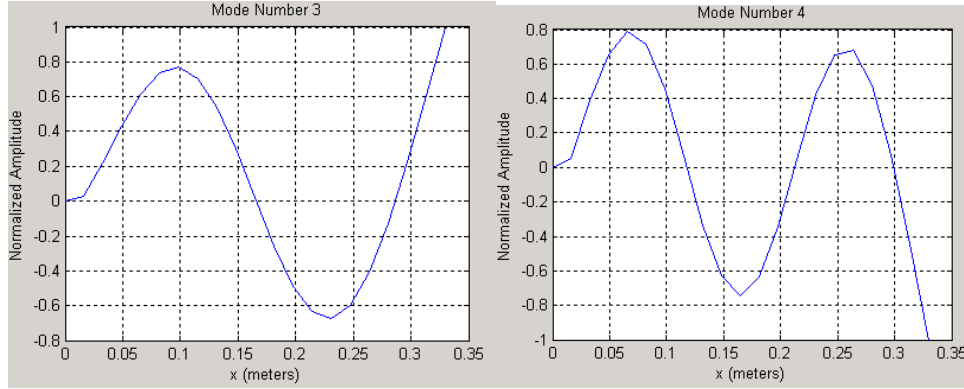


Figure 2-4: First Four Modeshapes

Figure 2-4 shows the first four modeshapes of the beam.

3 Solving the Eigenvalue Problem With Modal Analysis

Now that the mass and stiffness matrices have been generated, we can use modal analysis to solve an eigenvalue problem and find the natural frequencies and modeshapes of the beam. If we assume $\alpha_i(t) = A_i e^{j\omega_i t}$, (2.7) takes the form:

$$Kx = \omega_i^2 Mx \quad (3.1)$$

If we premultiply (2.12) by M^{-1} , we get $M^{-1}Kx = \omega_i^2 x$ which is of the form $Ax = \lambda x$.

Thus we can solve the characteristic equation $|M^{-1}K - I\omega_i^2| = 0$ and arrive at the natural frequencies of the beam. Once the natural frequencies are known, it is a relatively straightforward process to find the modeshapes. If we denote the i^{th} modeshape as \vec{X}_i , then the vibrations of the beam will be $\vec{x} = \vec{X}_1\alpha_1(t) + \vec{X}_2\alpha_2(t) + \dots + \vec{X}_{N-2}\alpha_{N-2}(t)$ which can be written as

$$\bar{x} = \begin{bmatrix} \bar{X}_1 & \bar{X}_2 & \cdots & \bar{X}_{N-2} \end{bmatrix} \begin{bmatrix} \alpha_1 \\ \alpha_2 \\ \vdots \\ \alpha_{N-2} \end{bmatrix} = \mathbf{X}\bar{\alpha} \quad (3.2)$$

Substituting (3.2) into (2.7) we have

$$M\mathbf{X}\ddot{\bar{\alpha}} + K\mathbf{X}\bar{\alpha} = B_0 \quad (3.3)$$

we can now use the property of orthogonality to reduce (3.3) to a series of single degree of freedom systems. We premultiply (3.3) by \mathbf{X}^T and get

$$\mathbf{X}^T M\mathbf{X}\ddot{\bar{\alpha}} + \mathbf{X}^T K\mathbf{X}\bar{\alpha} = \mathbf{X}^T B_0 \quad (3.4)$$

Because X_i and X_j are orthogonal with respect to the mass and stiffness matrix when

$i \neq j$, $M_{gen} = \mathbf{X}^T M\mathbf{X}$ becomes a diagonal matrix of the form

$$M_{gen} = \begin{bmatrix} m_1 & 0 & \cdots & 0 \\ 0 & m_2 & \ddots & \vdots \\ \vdots & \ddots & \ddots & 0 \\ 0 & \cdots & 0 & m_{N-2} \end{bmatrix} \quad (3.5)$$

where m_1, m_2, \dots, m_{N-2} are the generalized modal mass terms. Similarly with the stiffness

matrix $K_{gen} = \mathbf{X}^T K\mathbf{X}$ we have

$$K_{gen} = \begin{bmatrix} k_1 & 0 & \cdots & 0 \\ 0 & k_2 & \ddots & \vdots \\ \vdots & \ddots & \ddots & 0 \\ 0 & \cdots & 0 & k_{N-2} \end{bmatrix} \quad (3.6)$$

where k_1, k_2, \dots, k_{N-2} are the generalized modal stiffness terms. The generalized mass and

stiffness terms are related to the natural frequencies in that

$$\omega_i^2 = \frac{k_i}{m_i} \quad (3.7)$$

The right-hand side of (2.15) $\mathbf{X}^T B_0$ represents the generalized modal force.

$$B_{0i} = X_i^T B_0 \quad (3.8)$$

Each modal response can therefore be written as a single degree of freedom system

$$\ddot{\alpha}_i + \omega_i^2 \alpha_i = \frac{B_{0i}}{m_i} \quad (3.9)$$

And the full multi-degree-of-freedom response is given by (3.2).

4 Controllability and Placement of Piezos

An important problem that arises is the placement of the piezos. We wish to optimize the controllability of the structure, thus it is important that we have an accurate measure of the controllability as a function of x . We are interested in the first five modes of the beam, so we will restrict our analysis to accommodate these modes.

4.1 Forcing Due to Piezos

For a beam forced by piezos, the governing equation is given by

$$\frac{\partial^2}{\partial x^2} \left(EI \frac{\partial^2 y}{\partial x^2} - C_a V_a \chi(x) \right) + \rho A \frac{\partial^2 y}{\partial t^2} = 0 \quad (4.1)$$

where $C_a = \frac{1}{2} E_a d_{13} w (t_a + t_b)$, E_a is the elastic modulus for the piezo, d_{13} is the electric charge constant of the film, w is the width of the piezo, t_a is the thickness of the piezo,

t_b is the thickness of the beam and $\chi(x) = \begin{cases} 1 & r_1 \leq x \leq r_2 \\ 0 & \text{otherwise} \end{cases}$ is a function defining the

position of the piezo [8]. Rewriting (4.1) we have

$$\frac{\partial^2}{\partial x^2} \left(EI \frac{\partial^2 y}{\partial x^2} \right) + \rho A \frac{\partial^2 y}{\partial t^2} = C_a V_a \chi''(x)$$

Applying the Galerkin formulation to the right hand side, and integrating by parts twice we arrive at

$$\begin{aligned} C_a V_a \int_0^L \chi''(x) \phi_i(x) dx &= C_a V_a \int_0^L \chi(x) \phi_i''(x) dx = C_a V_a \int_{r_1}^{r_2} \phi_i''(x) dx \\ &= C_a V_a \left[\phi_i'(r_2) - \phi_i'(r_1) \right] \end{aligned} \quad (4.2)$$

Thus the full Galerkin formulation for the dynamic equations will be

$$M\mathbf{X}\ddot{\bar{\alpha}} + K\mathbf{X}\bar{\alpha} = B_0 \quad (4.3)$$

where $B_{0i} = C_a V_a \left[\phi_i'(r_2) - \phi_i'(r_1) \right]$.

4.2 Controllability

We first put the dynamic equations into their first order state-space open loop realization:

$$\begin{aligned} M\dot{x} + Kx &= B_0 u \\ x_1 &= x \\ x_2 &= \dot{x} \\ \dot{x}_1 &= x_2 \\ \dot{x}_2 &= -M^{-1}Kx_1 + B_0 u \end{aligned}$$

Therefore

$$\begin{pmatrix} \dot{x}_1 \\ \dot{x}_2 \end{pmatrix} = \begin{bmatrix} \mathbf{0}^{(N-2 \times N-2)} & I^{(N-2 \times N-2)} \\ -M^{-1}K & \mathbf{0}^{(N-2 \times N-2)} \end{bmatrix} \begin{pmatrix} x_1 \\ x_2 \end{pmatrix} + \begin{bmatrix} \mathbf{0}^{(N-2 \times 1)} \\ B_0 \end{bmatrix} C_a V_a$$

which is of the form $\dot{x} = Ax + Bu$ [†]. It can be shown that if a positive definite matrix P exists that satisfies the equation $PA + A^T P + BB^T = 0$ [12], then the system is controllable. The task then becomes finding the position in which to place the piezo, which will result in the greatest controllability for the first five modes. A measure of “how” positive definite P is to take the trace of P . If P has a large trace then the system will have high controllability, thus the goal is to find the location on the beam which will result in the largest trace of P . A simulation is run in Matlab to find the trace of P for all locations. Figure 4.1 shows the trace of P vs. the center of the piezo along the beam.

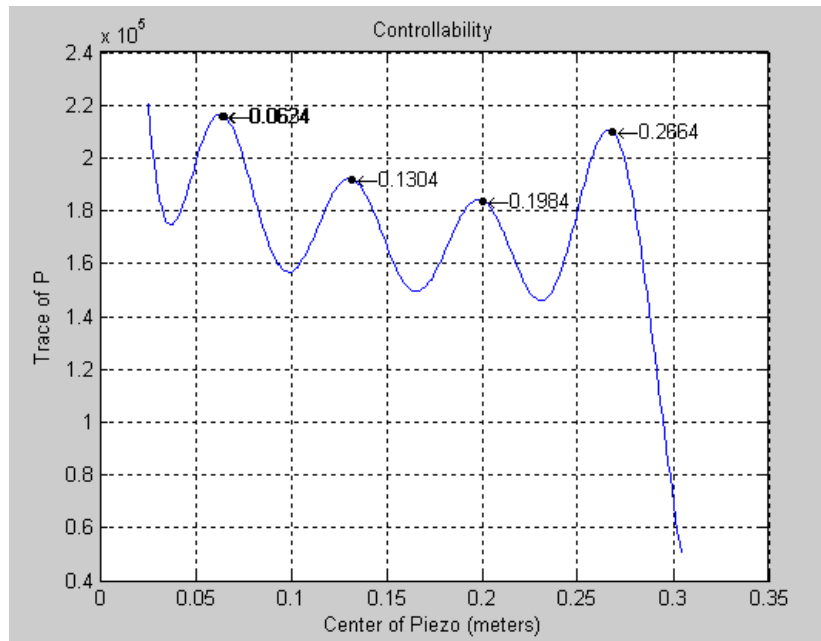


Figure 4-1: Trace of P vs. Center of Piezo

From the figure we see that the location of highest controllability is at the root of the beam with several peaks following. The optimal location for the collocated pair of piezos was determined to be the root of the beam and a second collocated pair was chosen to be placed at $x = 0.1304$ meters from the root to be used in future experiments.

[†] Note: B in the state-space realization should not be confused with B_0 which is the forcing vector

5 Response to Forcing

Now that we have a method for modeling the vibrations in a cantilever beam, we test the validity of the model with the Impact Hammer test. Ideally this is the impulse response, but in reality, it is impossible to achieve a pure impulse. In this chapter we investigate the ideal impulse response, and extend the theory to model the actual forcing function produced by the impact hammer.

5.1 Impulse Response

The right hand side of (2.6) is the forcing vector. With an ideal impulse, the forcing function $f(x,t) = F_0 \delta(x-a) \delta(t-t_0)$ where a is the location of the impact, t_0 is the time of impact and F_0 is the intensity of the impact. Substituting this into the right hand side of (2.6), we have

$$B_0 = \left\{ \begin{array}{c} \int_0^L \phi_1(x) \delta(x-a) dx \\ \int_0^L \phi_2(x) \delta(x-a) dx \\ \vdots \\ \int_0^L \phi_{N-1}(x) \delta(x-a) dx \\ \int_0^L \phi_N(x) \delta(x-a) dx \end{array} \right\} F_0 \delta(t-t_0) \quad (5.1)$$

When (5.1) is evaluated, we have

$$B_0 = \begin{Bmatrix} \phi_1(a) \\ \phi_2(a) \\ \vdots \\ \phi_{N-1}(a) \\ \phi_N(a) \end{Bmatrix} F \delta(t-t_0) \quad (5.2)$$

We now substitute (5.2) into (3.4) to decouple the mass and stiffness matrices and get the modal response:

$$B_{0i} = X_i^T \begin{Bmatrix} \phi_1(a) \\ \phi_2(a) \\ \vdots \\ \phi_{N-1}(a) \\ \phi_N(a) \end{Bmatrix} B_0 \quad (5.3)$$

For the i^{th} mode, we set up the SDOF system as follows

$$m_i \ddot{\alpha}_i + k_i \alpha_i = B_{0i} \delta(t-t_0)$$

The term B_{0i} is handled as an impulse and we use the classic example $B_{0i} \Delta t = m_i \dot{\alpha}_i(t_0)$ (assuming the beam is at rest prior to impact). We then treat the problem as a free-vibration case with the following initial conditions: $\alpha_i(t_0) = 0$ and

$\dot{\alpha}_i(t_0) = \frac{B_{0i} \delta(t-t_0)}{m_i} = \frac{I_i}{m_i}$ where $I_i = B_{0i} \delta(t-t_0)$. The impulse response for the i^{th} mode

is thus

$$\alpha_i(t) = \left\{ \frac{I_i}{m_i \omega_i} \sin(\omega_i [t-t_0]) \right\} u(t-t_0) \quad (5.4)$$

and the full MDOF response of the system is given by (3.2).

5.2 Duhamel's Integral

Because the true forcing function cannot be modeled as an ideal impulse, we must conceive of more practical methods of modeling the true response of the system.

Consider the forcing function shown in Figure 5-1.

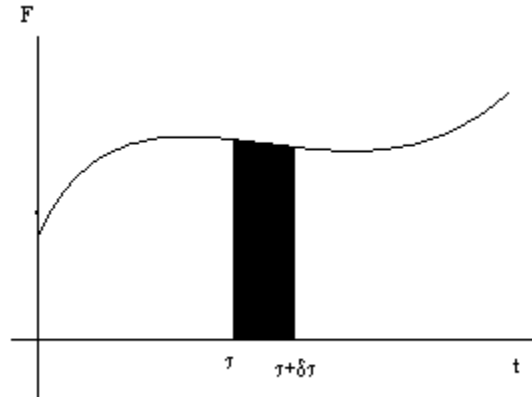


Figure 5-1: Force vs. Time

If we consider the response of the beam due to just the portion of the forcing function that is highlighted and allow $\delta\tau \rightarrow 0$, we notice that the term $F(\tau)\delta\tau$ approaches the definition of an impulse. Thus the response of the beam due to this infinitesimal interval is

$$d\alpha_i(t) = \frac{F(\tau)_i}{m_i\omega_i} \sin(\omega_i[t - \tau]) d\tau \quad (5.5)$$

Thus by the Superposition Principle, we are permitted to integrate over τ to get the full response:

$$\alpha_i(t) = \frac{1}{m_i\omega_i} \int_0^t F(\tau)_i \sin(\omega_i[t - \tau]) d\tau \quad (5.6)$$

Equation (5.6) is known as Duhamel's Convolution Integral. Although it is quite cumbersome in most cases, it is a very powerful tool for finding the modal response due to complicated forcing functions, and is relatively simple to apply numerically.

5.3 Response From Impact Hammer

With the *PCB Piezotronics* Impact Hammer model GK291D02, we are able to strike the beam and output the force of the impact as a function of time. The beam was struck at approximately the free end ($x=0.33\text{m}$) and the force of impact was saved to a file. Using the program *Impulse.m*, we are able to read from this file and apply Duhamel's Convolution Principle to simulate the response of the beam. Figure 5-2 shows the forcing function with time and Figure 5-3 shows the simulated response of the beam due to the impact hammer:

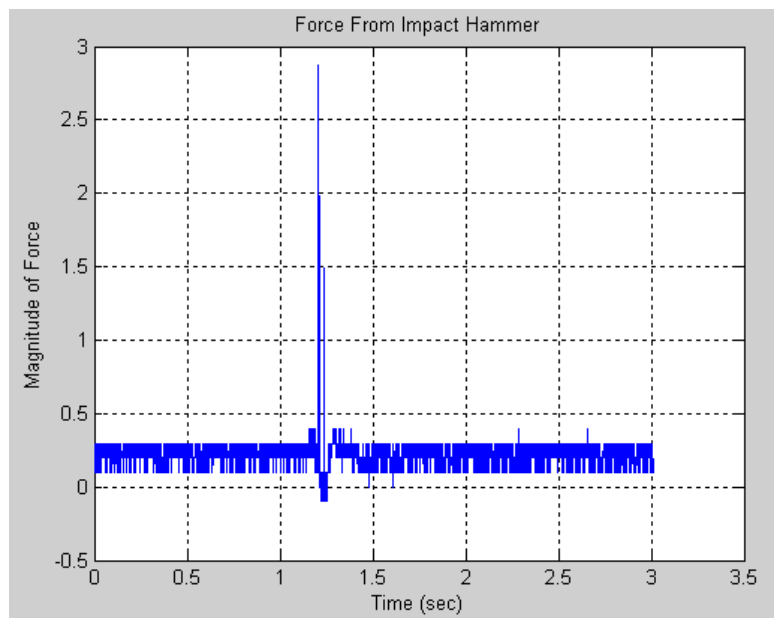


Figure 5-2: Force From Hammer

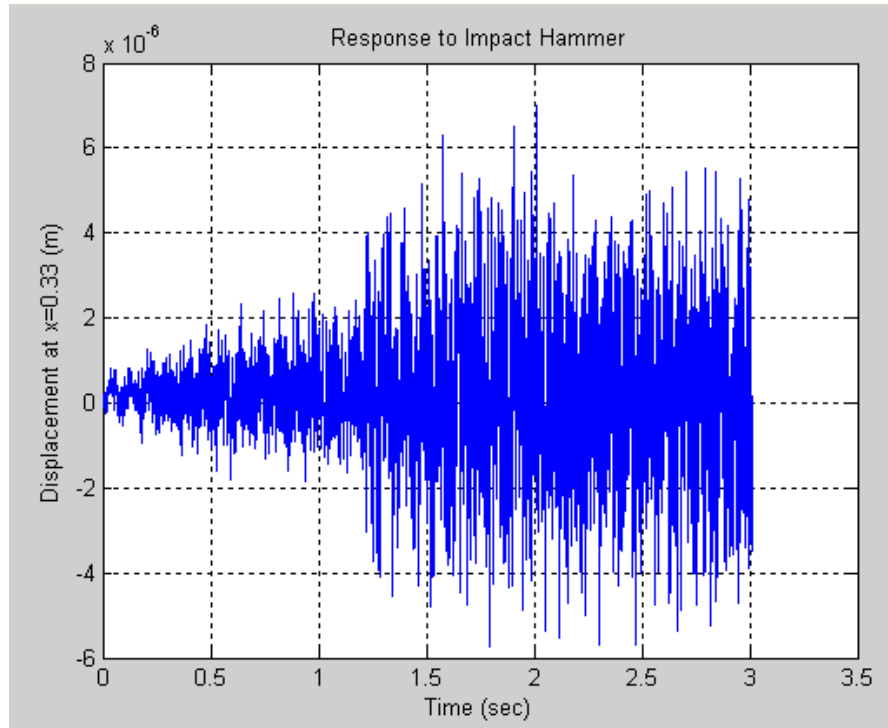


Figure 5-3: Response From Impact Hammer

The beam was struck at approximately $t=1.25$ seconds, and it is clear that the vibrations jump in amplitude at this time, however there is still a simulated response for $t \leq 1.25$, while the beam was at rest during this time. This is due to noise from the hammer. It is observed in Figure 5-2 that although there was no force exerted on the beam prior to 1.25 seconds, the forcing function is still a small nonzero number and thus the simulation interprets it as force.

6 Damping

Thus far, we have not considered damping in any of our formulations. Unfortunately, it is very difficult to model damping especially because the damping matrix D does not necessarily share the convenient orthogonality property that the mass and stiffness

matrices have. Therefore, it is impossible to decouple the equations and solve the MDOF system as a series of SDOF systems. A common model for the damping matrix [14] is

$$D = \alpha_1 M + \alpha_2 K \quad (6.1)$$

where $\alpha_1 = 10 \times 10^{-5}$ and $\alpha_2 = 10 \times 10^{-3}$. This model preserves orthogonality, but there arise many stability issues. When damping is considered, the impulse response of the system becomes

$$\alpha_i(t) = \left\{ \frac{I_i}{m_i \omega_{di}} e^{-\zeta_i \omega_i t} \sin(\omega_{di} [t - t_0]) \right\} u(t - t_0) \quad (6.2)$$

and the Duhamel Integral becomes

$$\alpha_i(t) = \frac{1}{m_i \omega_{di}} \int_0^t F(\tau)_i e^{-\zeta_i \omega_i t} \sin(\omega_{di} [t - \tau]) d\tau \quad (6.3)$$

where $\zeta_i = \frac{\alpha_1}{2\omega_i} m_i + \frac{\alpha_2}{2\omega_i} k_i$ is the damping constant and $\omega_{di} = \omega_i \sqrt{1 - \zeta_i^2}$. Thus, if $\zeta_i^2 \geq 1$

the system will be unstable. In fact, when this model is applied to our system, we do experience instability and therefore this model cannot be used. Eventually, we will find the damping constants corresponding to each mode using analysis in the frequency domain when we generate the Bode plot, but for now damping is not considered.

7 Modeling Damping in the Frequency Domain

Now that we have an accurate model for the mass and stiffness matrices, we model the damping matrix, which will be crucial to the control synthesis. Damping in this model is considered as a linear combination of the mass and stiffness matrices as in (6.1). To solve for α_1 and α_2 we generate the experimental and computational frequency responses. The

resonant peaks of the magnitude response of the transfer function in consideration are measured experimentally using a HP 35670 Dynamic Signal Analyzer and compared to the computational peaks. The coefficients α_1 and α_2 are then optimized with the built-in minimization function *fmincon* in MATLAB®. The RMS error is minimized to 5.03 dB and the experimental vs. computational frequency response is shown in Figure 7-1.

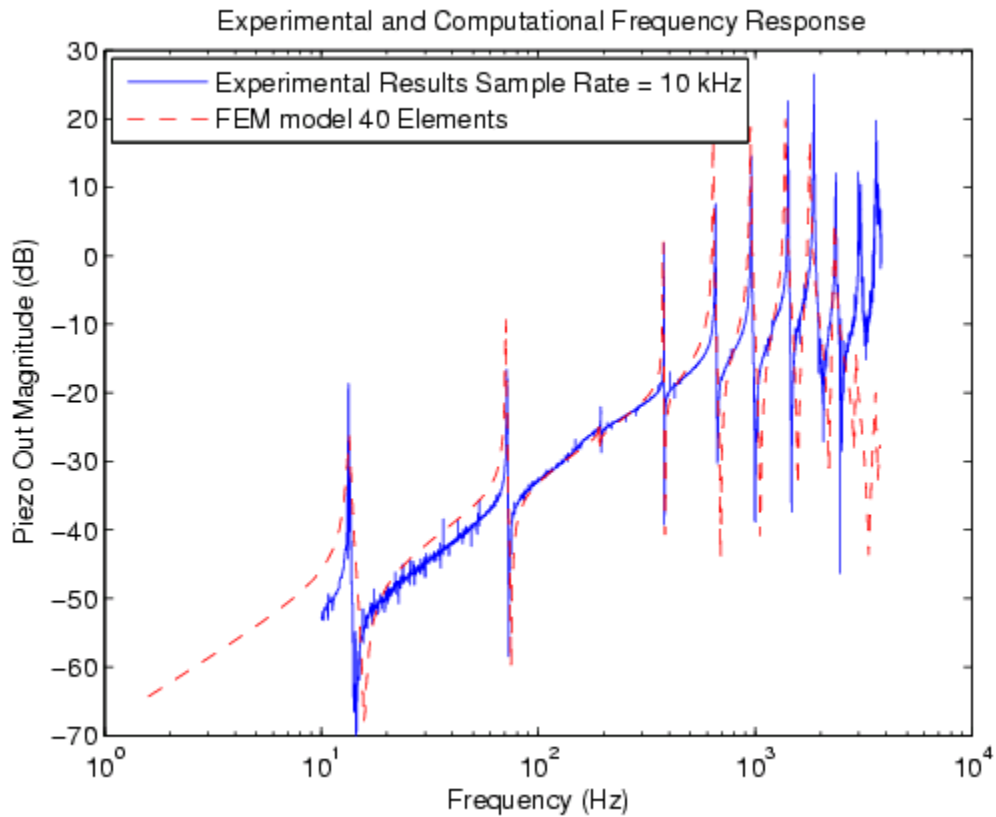


Figure 7-1: Experimental and Computational Frequency Response

8 The Control Synthesis Problem

Now that we have an acceptable computational model for the second order system, a control law is proposed for the first-order state-space realization of the damped system.

$$M\ddot{x} + D\dot{x} + Kx = B_0u \quad (8.1)$$

As in the undamped case (8.1) is put into its first order state-space open-loop realization

$$\dot{x} = \begin{bmatrix} 0 & I \\ -M^{-1}K & -M^{-1}D \end{bmatrix} x + \begin{bmatrix} 0 \\ M^{-1}B_0 \end{bmatrix} u \quad (8.2)$$

8.1 Feedback From the PZT

To close the loop, we make use of the sensor capabilities of the PZT. Collocated with the PZT actuator is a second PZT, which will be used as a sensor. The sensor will return a signal according to (8.3)

$$y = \begin{bmatrix} B_0^T & 0 \end{bmatrix} x \quad (8.3)$$

If we write the SISO transfer function for this system $T(s) = \frac{Y}{X}$ we observe that we have

a symmetric transfer function i.e. $T(s) = T^T(s)$

$$T(s) = B_0^T (Ms^2 + Ds + K)^{-1} B_0 \quad (8.4)$$

For the purposes of this investigation we are interested in *externally* symmetric transfer functions which implies that there is a nonsingular matrix L such that

$$A^T L = LA$$

and

$$C^T = LB$$

To achieve the external symmetry, it is necessary to differentiate the PZT output with respect to time. This is accomplished with an analog differentiator as described in later sections. Once the PZT output is differentiated, the feedback becomes

$$\dot{y} = \begin{bmatrix} 0 & B_0^T \end{bmatrix} x \quad (8.4)$$

and the open-loop transfer function is

$$T(s) = B_0^T s (Ms^2 + Ds + K)^{-1} B_0 \quad (8.5)$$

It is shown by inspection that external symmetry implies symmetry, but the converse is not true.

8.2 Feedback Control Law

For the control design, a method for calculating the H_∞ norm is required. The H_∞ norm is defined as follows

$$\|T(s)\|_\infty = \sup_{\omega \in \mathbb{R}} \sigma_{\max} \{ |T(j\omega)| \} \quad (8.6)$$

The standard method for calculating this value is to bring the system to its first order form and approximate the norm iteratively with a tedious and computationally demanding scheme requiring the solution of non-convex bilinear matrix inequalities with coupling rank constraints. With the system in consideration, however, we are able to exploit the external symmetry to approximate the H_∞ norm *explicitly* using an analytical upper bound method [5]. For an externally symmetric second order system, the H_∞ norm satisfies

$$\|T(s)\|_\infty < \gamma_0 = \lambda_{\max} (B_0^T D^{-1} B_0) \quad (8.7)$$

If a feedback control law of the following form is proposed

$$u = -G\dot{y} \quad (8.8)$$

the closed-loop transfer function will be

$$T(s) = B_0^T s (Ms^2 + (D + B_0^T G B_0)s + K)^{-1} B_0 \quad (8.9)$$

and the closed-loop H_∞ norm will be bound by the effective damping matrix $D + B_0^T G B_0$

$$\|T(s)\|_{\infty CL} < \gamma_0 = \lambda_{\max} \left(B_0^T (D + B_0^T G B_0)^{-1} B_0 \right) \quad (8.10)$$

With (8.10) we can solve algebraically for G [17] to set a closed-loop upper bound for the H_∞ norm of any desired value.

a) If B_0 is square and invertible then G can be selected as

$$G \geq \frac{1}{\gamma_0} I - B_0^{-1} D B_0^{-1T} \quad (8.11)$$

b) If $B_0^T B_0$ is singular then G can be selected as

$$G \geq B_0^+ \left[D B_0^{\perp T} (B_0^\perp D B_0^{\perp T})^{-1} B_0^\perp D - D + \frac{1}{\gamma} B_0 B_0^T \right] B_0^{+T} \quad (8.12)$$

Calculating G according to (8.11) or (8.12) guarantees the closed loop system an H_∞ norm less than γ .

8.3 Simulated Results

Now that we have an open-loop response that closely matches the experimentally measured frequency response, we can close the loop by feeding back the gain G calculated by (8.12). Setting γ equal to 10, 1 and .1 and feeding back the gain G calculated by (8.12), we get the following magnitude responses shown in Figures 8-1 through 8-3

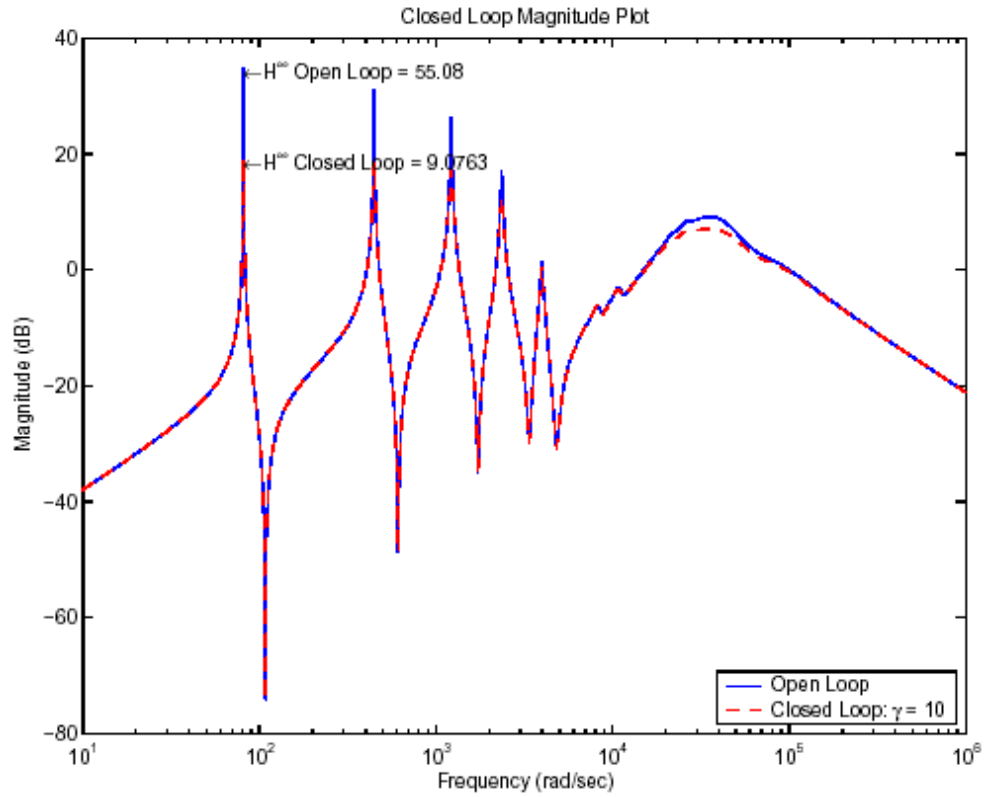


Figure 8-1: Closed Loop Frequency Response $\gamma=10$

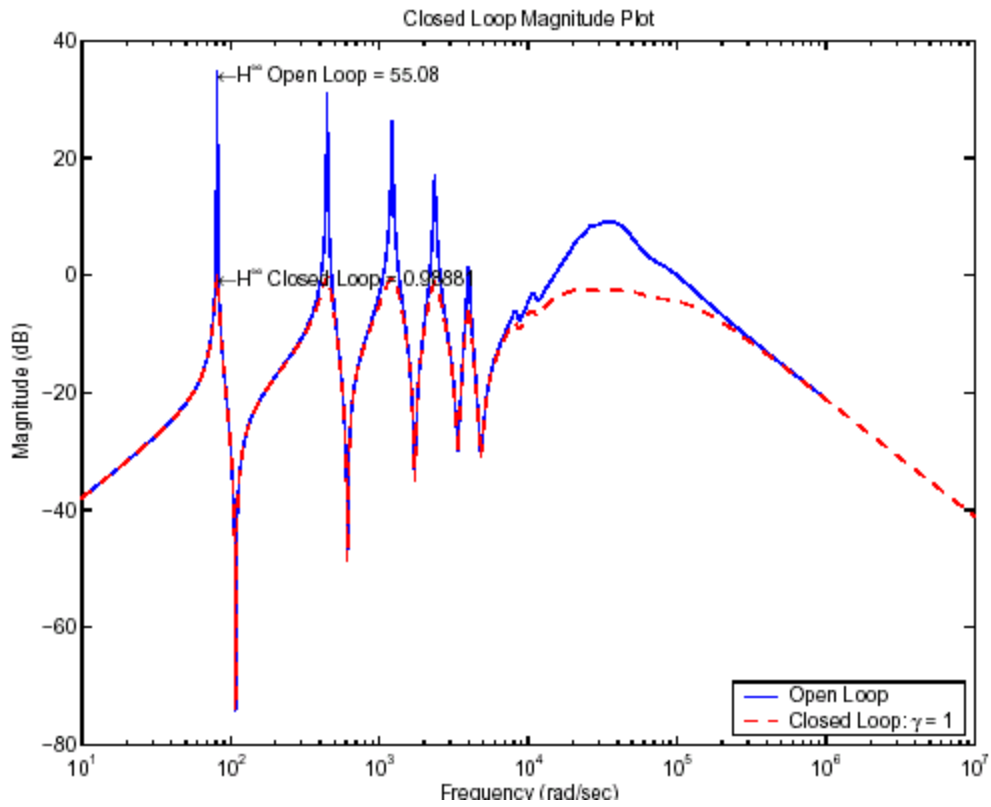


Figure 8-2: Closed Loop Frequency Response $\gamma=1$

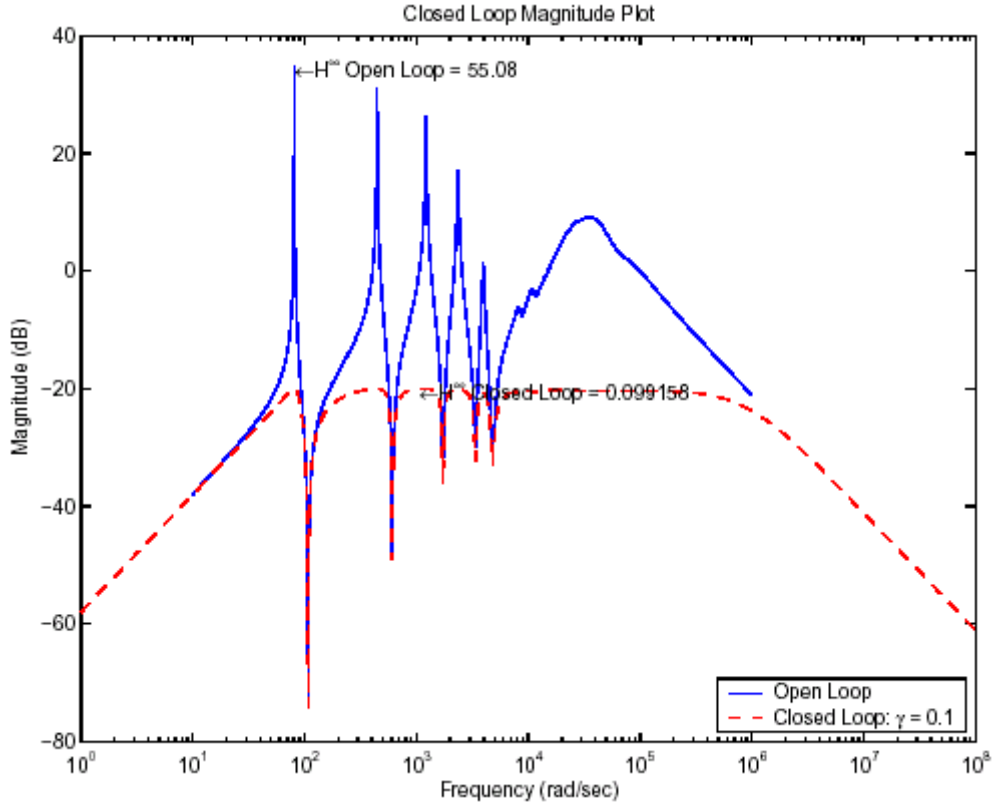


Figure 8-3: Closed Loop Frequency Response $\gamma=0.01$

Note that the closed-loop H_∞ norm in each case is sharply bounded by γ which is calculated by (8.10). For this particular system, the upper bound ostensibly is an accurate approximation for the actual H_∞ norm with immense computational savings. Table I shows the computer time necessary to calculate the upper bound using (8.10) vs. the computer time spent calculating the true norm using singular value decomposition and bisection methods.

Table II: Computation Time for Calculating the True Infinity Norm vs. (8.10) $n=120$

<i>True H_∞ Norm</i>		<i>Approximate Using (8.10)</i>	
CPU Time	True H_∞ Norm	CPU Time	Upper Bound
7.188	0.099105	0.016	0.1

A comparison between the static controller and the full state observer based controller is shown in Figure 8-4.

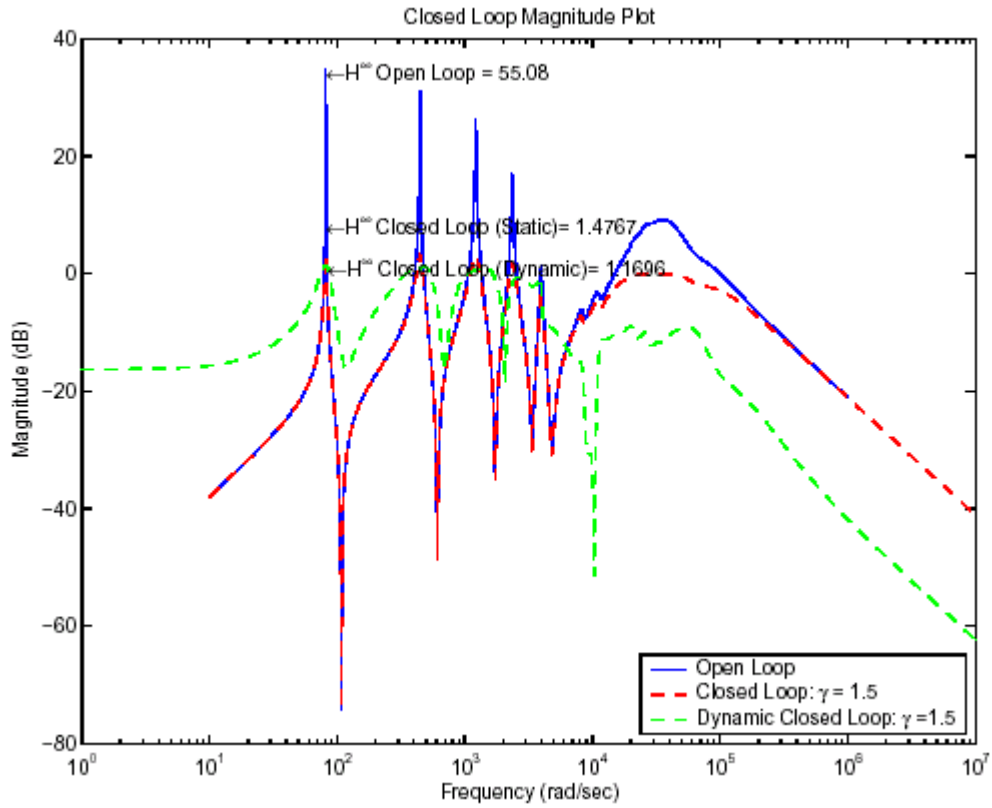


Figure 8-4: Magnitude plots using dynamic and static controllers $\gamma = 1.5$

The dynamic controller performs better than the static controller, but the small difference in performance is a small price to pay for the enormous computational savings provided by the static controller. Table III shows the computation time for the dynamic and static controllers as the computational model becomes more and more complicated.

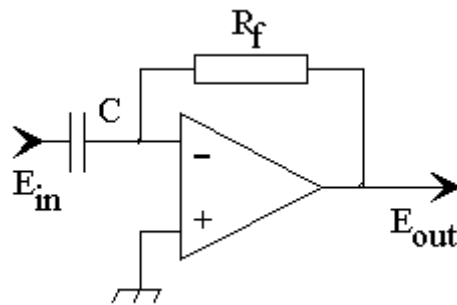
Table III: Computation Time for Dynamic and Static Controllers for $\gamma=1.5$

<i>Case</i>	<i>Dynamic</i>		<i>Static</i>	
# Elements	Time (seconds)	True norm	Time (seconds)	True norm
20	0.533	1.1696	0.047	1.4767
60	11.956	1.1693	0.531	1.4765
120	82.652	1.2236	3.875	1.4785

It is clear the static method is far more efficient than the dynamic in terms of numerical intensity. It also provides advantages in the simplicity of the controller. The controller is simply one gain G as opposed to a controller of length n required by the dynamic full state. The dynamic controller also requires a full state observer, which requires online computation and can force the user to lower the sample rate of the control loops. The static controller on the other hand can sample at extremely high rates.

9 Experimental Verification

Now that we have verified the theory with simulations, it is appropriate to verify the theory experimentally. First the system must be made externally symmetrical in order to employ (8.10). The output signal must therefore be differentiated in time using an analog differentiator as shown in Figure 9-1.

**Figure 9-1: Analog Differentiator DC Gain -40dB**

This differentiator is cascaded with a 5 kHz Butterworth Low-Pass anti-aliasing filter to produce the magnitude response shown in Figure 9-2.

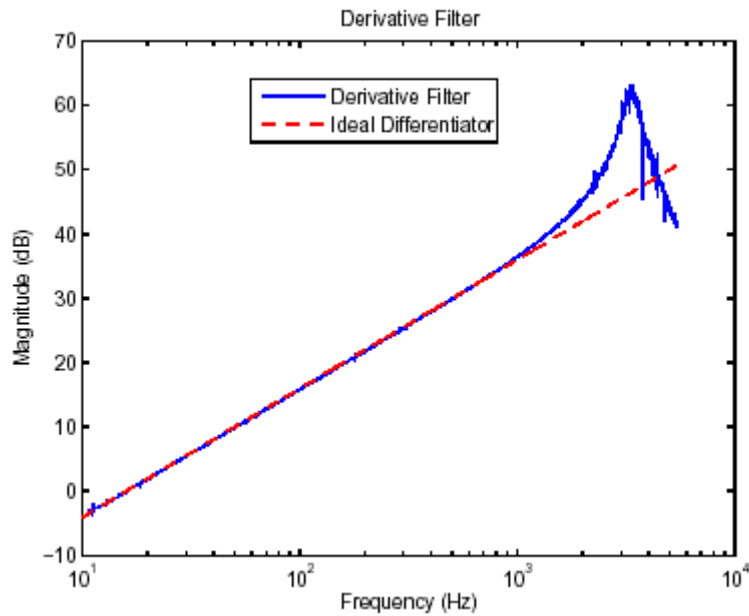


Figure 9-2: Magnitude Response of Analog Differentiator

The phase response is shown in Figure 9-3.

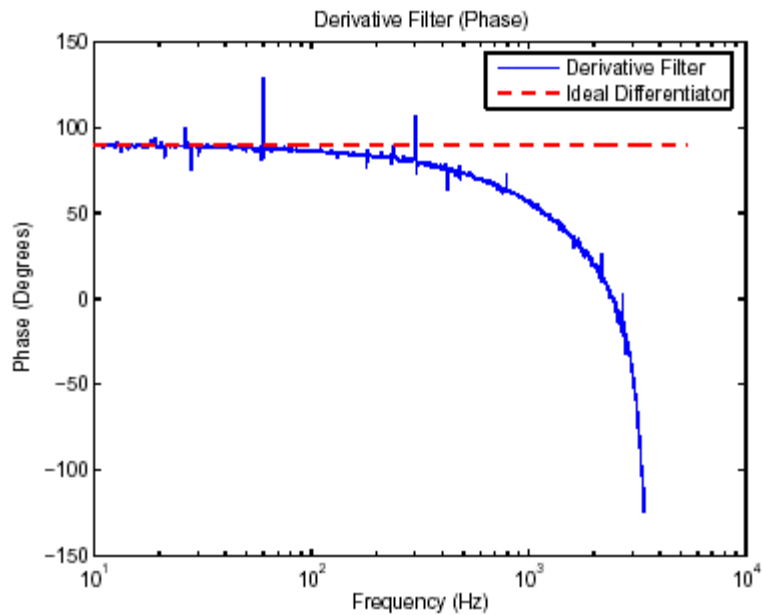


Figure 9-3: Phase Response of Analog Differentiator

As can be observed from Figures 9-3 and 9-4, the accuracy of the differentiator drops as $\omega \rightarrow \infty$. This is due to the anti-aliasing filter.

The experimental setup is shown in Figures 9-5, 9-6 and 9-7.

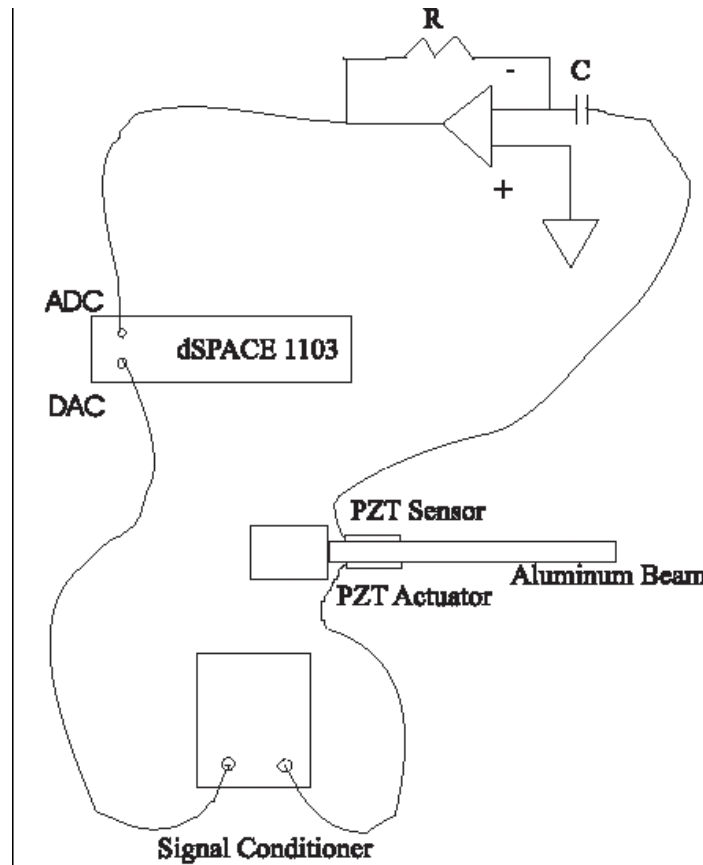


Figure 9-4: Schematics for the Apparatus



Figure 9-5: The Cantilevered Beam



Figure 9-6: dSPACE 1103 Rapid Prototyping Board + Differentiator

9.1 Experimental Results

In this section the experimental results will be compared with the computational results of choosing an arbitrary value for γ . For this experiment a closed-loop value of 17.61 was chosen for γ which corresponds to a 20 % reduction in the H_∞ norm from the open-loop.

Using (8.12) the static feedback gain is calculated to be $G = 0.055268$. Figure 9-7 shows

the simulated magnitude response of this closed-loop controller and Figure 9-6 shows the experimental results when the beam is excited with random noise.

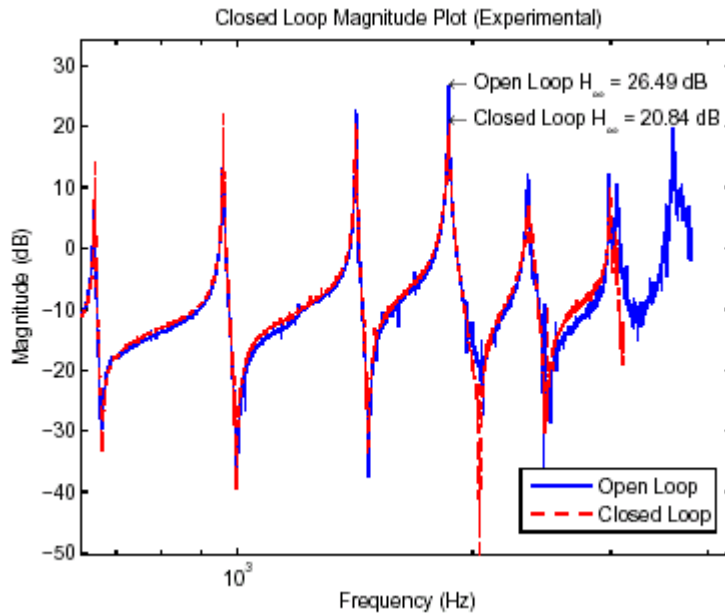


Figure 9-7: Open Loop and Closed Loop Magnitude Response $G = 0.055268$ (Experimental)

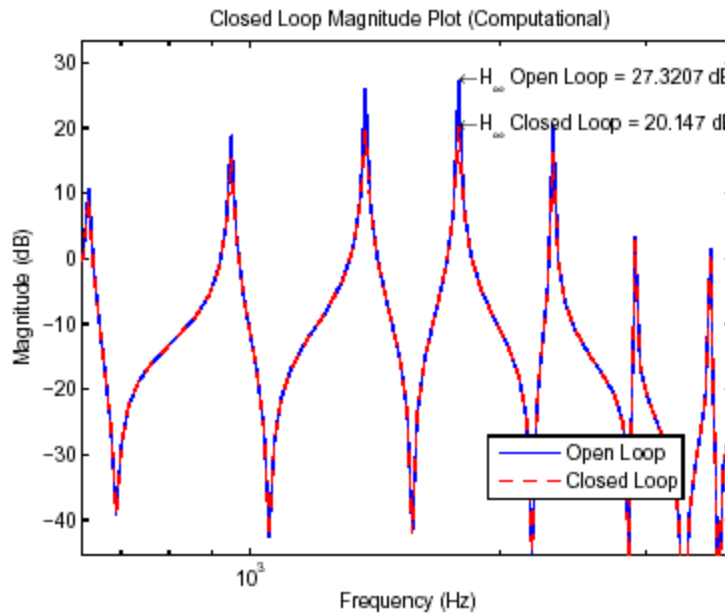


Figure 9-8: Open Loop and Closed Loop Magnitude Response $G = 0.055268$ (Computational 40 Elements)

10 Conclusions

From the results presented in sections 8 and 9, it is clear that the H_∞ control design using the analytic upper bound method has profound advantages over the full state dynamic controller in terms of computational efficiency, although it has limitations in its availability. The analytical upper bound method can only be used for externally symmetric transfer functions. When applicable, however, the static controller requires minimal computational complexity and is trivial to implement in real-time.

A Bibliography

- [1] H.T. Banks, R.C. Smith, and Y. Wang, *Smart Material Structures: Modeling, Estimation and Control*, Wiley-Masson, New York, 1996.
- [2] S. Boyd, V. Balakrishnan, and P. Kabamba, *A Bisection method for computing the H_∞ norm of a transfer function and related problems*, Mathematics of Control, Signals, and Systems, 2 (1989), pp. 207-219.
- [3] L. Meirovitch, *Computational Methods in Structural Dynamics*, Sijthoff and Noordhoff, Alphen aan den Rijn, The Netherlands, 1980.
- [4] R.E. Skelton, T. Iwasaki, and K. Grigoriadis, *A Unified Algebraic Approach to Linear Control Design*, Taylor & Francis, London, UK, 1998
- [5] K. Tan and K.M. Grigoriadis, *Stabilization and H_∞ control of symmetric systems: An Explicit Solution*, Systems & Control Letters, 44 (2001), pp. 57-72.
- [6] M.A. Demetriou and K.M. Grigoriadis, *Collocated actuator placement in structural systems using an analytical bound approach*, in Proceedings of the 2004 American Control Conference, Boston, MA, June 30-July 2 2004, pp. 1604-1609
- [7] P. Prenter, *Splines and Variational Methods*, Wiley-Interscience, New York, 1975.
- [8] A. Preumont, *Vibration Control of Active Structures: An Introduction*, Wiley-Interscience, New York, 1975.

- [9] S.O. Reza Moheimani, *Experimental Verification of the Corrected Transfer Function of a Piezoelectric Laminate Beam*, IEEE Transactions on Control Systems Technology, Vol. 8, No. 4, July 2000.
- [10] Dunant Halirn and S.O. Reza Moheimani, *Spatial H_2 Control of a Piezoelectric Laminate Beam: Experimental Implementation*, IEEE Transactions on Control Systems Technology, Vol. 8, No. 4, July 2002.
- [11] Dunant Halirn and S.O. Reza Moheimani, *Experimental Implementation of Spatial H_∞ Control on a Piezoelectric-Laminate Beam*, IEEE Transactions on Control Systems Technology, Vol. 7, No. 3, September 2002.
- [12] K. Zhou with John C. Doyle, *Essentials of Robust Control*, Prentice Hall New Jersey, 1998.
- [13] S.O.R. Moheimani, Dunant Halim & Andrew J. Fleming, *Spatial Control of Vibrations: Theory and Experiments*, World Scientific, Series A, Vol. 10, 2003.
- [14] Jer-Nan Juang and Minh Q. Phan, *Identification and Control of Mechanical Systems*, Cambridge University Press, 2001.
- [15] P.R. Belanger, *Control Engineering: A Modern Approach*, Saunders College Publishing, 1995.
- [16] Y. Bai, K.M. Grigoriadis, and M.A. Demetriou, “ H_∞ collocated control of structural systems: An analytical bound approach,” in *Proceedings of the 2004 American Control Conference*, pp. 2081-2086, (Boston, MA), June 30- July 2 2004.

- [17] R.J. Sweeney, M.A. Demetriou, and K.M. Grigoriadis, “ H_∞ control of a piezo-actuated flexible beam using an analytical bound approach,” in *Proceedings of the 2005 American Control Conference*, (Portland, OR), June 8-10 2005.
- [18] M.H. Schultz, *Spline Analysis*, Prentice Hall, Englewood Cliffs, N.J., 1973.
- [19] D.J. Inman, *Vibration With Control, Measurement and Stability*, Prentice Hall, Englewood Cliffs, N.J., 1989.
- [20] L. Meirovitch, *Dynamics and Control of Structures*, John Wiley and Sons, Inc., New York, 1990.
- [21] H.T. Banks and K. Kunisch, *Estimation Techniques for Distributed Parameter Systems*, Birkhauser, Boston, 1989.